Lifetimes of the 4_1^+ states of ^{206}Po and ^{204}Po: A study of the transition from noncollective seniority-like mode to collectivity

M. Stoyanova,[1] G. Rainovski,[1,*] J. Jolie,[2] N. Pietralla,[3] A. Blazhev,[2] M. Beckers,[2] A. Dewald,[2] M. Djongolov,[1] A. Esmaylzadeh,[2] C. Fransen,[2] L. M. Gerhard,[2] K. A. Gladnishki,[1] S. Herb,[2] P. R. John,[3] V. Karayonchev,[2] J. M. Keatings,[4] R. Kern,[3] L. Knafla,[2] D. Kocheva,[1] L. Kornwebel,[2] Th. Kröll,[3] M. Ley,[2] K. M. Mashtakov,[4] C. Müller-Gatermann,[2] J.-M. Régis,[2] M. Scheck,[4] K. Schomacker,[2] J. Sinclair,[4] P. Spagnoletti,[4] C. Sürder,[3] N. Warr,[2] V. Werner,[3] and J. Wiederhold[3]

[1]*Faculty of Physics, St. Kliment Ohridski University of Sofia, 1164 Sofia, Bulgaria*

[2]*Institut für Kernphysik, Universität zu Köln, 50937 Köln, Germany*

[3]*Institut für Kernphysik, Technische Universität Darmstadt, 64289 Darmstadt, Germany*

[4]*School of Computing, Engineering, and Physical Sciences, University of the West of Scotland, Paisley PA1 2BE, United Kingdom*

(Received 7 October 2019; published 6 December 2019)

Low-lying yrast states of ^{204}Po and ^{206}Po were investigated by the γ-γ fast timing technique with $LaBr_3$(Ce) detectors. Excited states of these nuclei were populated in the ^{197}Au(^{11}B, $4n$)^{204}Po and the ^{198}Pt(^{12}C, $4n$)^{206}Po fusion-evaporation reactions, respectively. The beams were delivered by the FN-Tandem accelerator at the University of Cologne. The lifetimes of the 4_1^+ states of both nuclei were measured, along with an upper lifetime limit for the 2_1^+ state of ^{204}Po. A comparison between the derived $B(E2; 4_1^+ \rightarrow 2_1^+)$ values and results from simplified empirical two-state mixing calculations suggests that for the 4_1^+ states of even-even polonium isotopes the transition from single-particle mode at $N = 126$ to collective mode, when reducing the number of neutrons, occurs above $N = 122$.

DOI: 10.1103/PhysRevC.100.064304

I. INTRODUCTION

The nuclear shell model represents the most fundamental concept in nuclear structure physics that naturally leads to the appearance of magic numbers due to the existence of large energy gaps, primarily defined by the shape of the potential and the spin-orbit interaction [1]. The shell model, in combination with pairing correlations, provides an easy way to understand low-energy spectra of semimagic nuclei. Low-energy excited states with $J > 0$ in semimagic nuclei, with more than one particle in a single high-j orbital, are formed by recoupling of angular momenta of unpaired nucleons, thus forming multiplets of states that have the same number of unpaired nucleons. This number is called seniority (ν) [2–4] and is generally considered as a good quantum number. In fact, the generalized seniority scheme [3,4] represents a truncation of the nuclear shell model. For the yrast states of even-even nuclei the seniority scheme is manifested by a few clear experimental signatures [5,6]: the excited yrast states have seniority $\nu = 2$ and follow an energy pattern that is equivalent to the one for a j^2 configuration in which the energy spacing between the states decreases towards the state with maximum angular momentum; the absolute $E2$ transition strength for the seniority-changing transition $2_1^+(\nu = 2) \rightarrow 0_1^+(\nu = 0)$ increases in a parabolic way with the filling of the j shell and reaches a maximum at the middle of the j shell; and the absolute $E2$ transition strengths for the seniority-conserving transitions $J \rightarrow J - 2 (J > 4)$ decrease in a parabolic way with the filling of the j orbital and reaches a minimum at the middle of the j orbital. It can be expected that the features of the seniority scheme persist in open-shell nuclei close to magic numbers in which low-energy excitations are dominated by nucleons of the same kind. However, when the number of the other kind of valence nucleons increases, it can also be expected that the proton-neutron interaction increases [7] and eventually a collective behavior emerges. In fact, this can be deemed as a transition from single-particle (seniority-type) excitations to collective ones. When and how this transition appears, i.e., to what extent the seniority features persist in open shell nuclei, is not entirely clear. A recent similar study for the $N = 50$ isotopes has shown that the breaking down of the seniority symmetry is caused by cross-shell core excitations [8].

The open-shell Po-Rn-Ra nuclei in the vicinity of the double-magic nucleus ^{208}Pb offer a suitable ground for studying the transition from single-particle seniority type excitations to collective mode. It can be expected, as suggested in Ref. [5], that the valence neutrons in $N \leqslant 126$ nuclei occupy orbitals with high principal quantum number and low angular momentum. As a result, they interact weakly with the protons in the $h_{9/2}$ orbital [9], which dominate the wave functions of the yrast states forming a seniority-like structure. Indeed, for all even-even nuclei in the Po-Rn-Ra isotonic chains with $122 \leqslant N \leqslant 126$ the yrast states follow a typical seniority-like pattern. The 8_1^+ states in these nuclei are isomers with wave functions dominated by the $\pi(h_{9/2})^n$ configuration [10]. The latter assignment is in agreement with the almost constant values of the measured magnetic moments of these

*rig@phys.uni-sofia.bg

states [11]. Moreover, the $B(E2; 8_1^+ \rightarrow 6_1^+)$ values decrease with the increase of proton number for all even-even nuclei in the Po-Rn-Ra isotonic chains with $120 \leqslant N \leqslant 126$ [5]. Based on these arguments Ressler *et al.* [5] suggested that the noncollective seniority regime persists for nuclei from the Po-Rn-Ra isotonic chains with $122 \leqslant N \leqslant 126$ up to ^{210}Ra [10], and a collective behavior emerges around $N = 118$–120.

However, it has to be noted that due to lack of experimental data, the interpretation in Ref. [5] does not include the evolution of the absolute $E2$ transition strengths for the seniority-changing transitions $2_1^+(\nu = 2) \rightarrow 0_1^+(\nu = 0)$. Recently $B(E2; 2_1^+ \rightarrow 0_1^+)$ values of 18^{+14}_{-10} W.u. and 13(6) W.u. have been reported for the $N = 122$ isotones ^{206}Po and ^{208}Rn, respectively [12]. These values suggest a constant, or slightly increasing trend with respect to the $B(E2; 2_1^+ \rightarrow 0_1^+)$ value in ^{204}Pb, instead of the expected more rapid increase, should the seniority regime persist. Based on this observation and QRPA calculations [12], it has been suggested that, at least for the 2_1^+ states of the polonium isotopes, a moderate collectivity sets in immediately when moving away from the closed proton shell [12]. Thus, the energy level pattern and the evolution of the $B(E2; 8_1^+ \rightarrow 6_1^+)$ values suggest that the noncollective seniority regime persists for the $N = 122$ isotones, as suggested in Refs. [5,10], while the newly measured values of the $B(E2; 2_1^+ \rightarrow 0_1^+)$ in ^{206}Po and ^{208}Rn indicate a moderate collectivity [12]. This suggests that the transition from single-particle seniority-type mode to collective mode develops differently for low- and high-spin states. In order to shed more light on this process we have measured the lifetimes of the 4_1^+ states of ^{206}Po and ^{204}Po which determine the $E2$ transition strengths for the seniority-preserving transition $4_1^+(\nu = 2) \rightarrow 2_1^+(\nu = 2)$. Until now, these data were missing due to experimental difficulties that stem from the fact that the 4_1^+ states of these nuclei are positioned between the long-lived 8_1^+ states [$\tau(8_1^+; ^{206}\text{Po}) = 335(6)$ ns [13] and $\tau(8_1^+; ^{204}\text{Po}) = 202(7)$ ns [14]] and the short-lived 2_1^+ states [$\tau(2_1^+; ^{206}\text{Po}) = 3.7^{+2.8}_{-1.7}$ ps [12]].

II. EXPERIMENT

The experiments were performed at the HORUS spectrometer [15] of the FN Tandem facility at the University of Cologne. The excited states of ^{206}Po were populated in the ^{198}Pt(^{12}C, $4n$) fusion-evaporation reaction at a beam energy of 65 MeV. The target used was a ^{198}Pt foil with a thickness of 10 mg/cm^2 enriched to 91.6%. The excited states of ^{204}Po were populated in the ^{197}Au(^{11}B, $4n$) fusion-evaporation reaction at a beam energy of 55 MeV. A 110-mg/cm^2-thick ^{197}Au foil was used as a target. The γ rays from the decay of the excited states were detected by a hybrid array consisting of eight HPGe detectors and nine $LaBr_3$(Ce) scintillators (hereafter called LaBr), each with dimensions ø1.5 × 1.5 in. To suppress the Compton background, six of the LaBr detectors were placed inside bismuth-germanate (BGO) anti-Compton shields. The other three LaBr had lead shields to suppress background events associated with scattered γ rays. The time differences between the timing signals for every unique combination of LaBr detectors were measured using time-to-amplitude converters (TAC) applying the multiplexed-start and multiplexed-stop electronics setup [16]. The detector energy signals and the TAC amplitudes were recorded using 80-MHz synchronized digitizers in a triggerless mode.

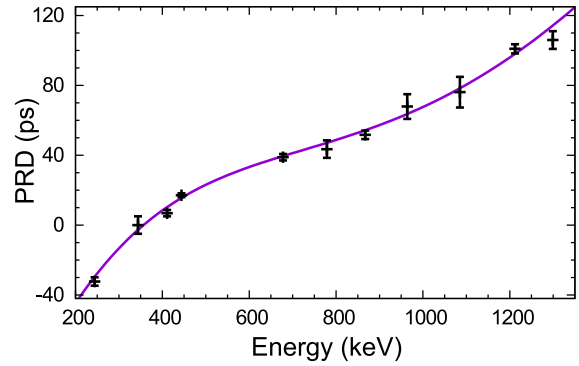

FIG. 1. The PRD curve of the setup measured with a ^{152}Eu source.

The lifetimes of the states of interest were extracted from the time difference spectra by applying the generalized centroid difference (GCD) method. The method is discussed in detail in Ref. [17]. Some aspects of the present analyses along with preliminary results are also presented in Ref. [18]. Here we briefly present the method and the final results from the analyses. In the GCD method, two independent time spectra are obtained, constructed as the time difference between two signals generated by two consecutive γ rays that populate and depopulate an excited state of interest. When a transition which feeds the state (E_f) provides the start signal to the TAC and a decay transition (E_d) from this state provides the stop signal, a time difference distribution labeled as "Delayed" (D) is obtained. In the reverse case, a time difference distribution labeled as "Antidelayed" (AD) is obtained. Both distributions are characterized by their centroids, C^{D} and C^{AD}, respectively. Assuming no background contributions, the mean lifetime of the state of interest τ can be expressed via the difference between the centroids of the time spectra:

$$\Delta C(E_f, E_d) \equiv C^D - C^{AD} = 2\tau + \text{PRD}(E_f, E_d). \quad (1)$$

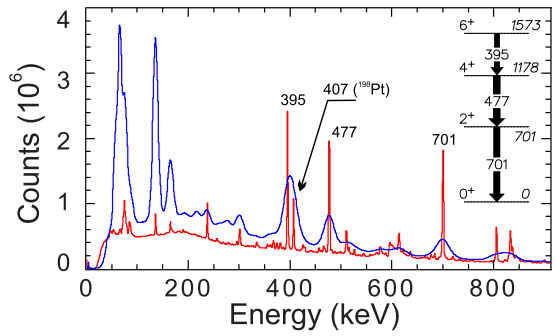

FIG. 2. Full projections of the HPGe-LaBr-LaBr (blue) and HPGe-LaBr-HPGe (red) coincidence data from the ^{198}Pt(^{12}C, $4n$) reaction at a beam energy of 65 MeV. The inset shows a partial level scheme of ^{206}Po. The peaks from the transitions used in the analyses are labeled by their energies.

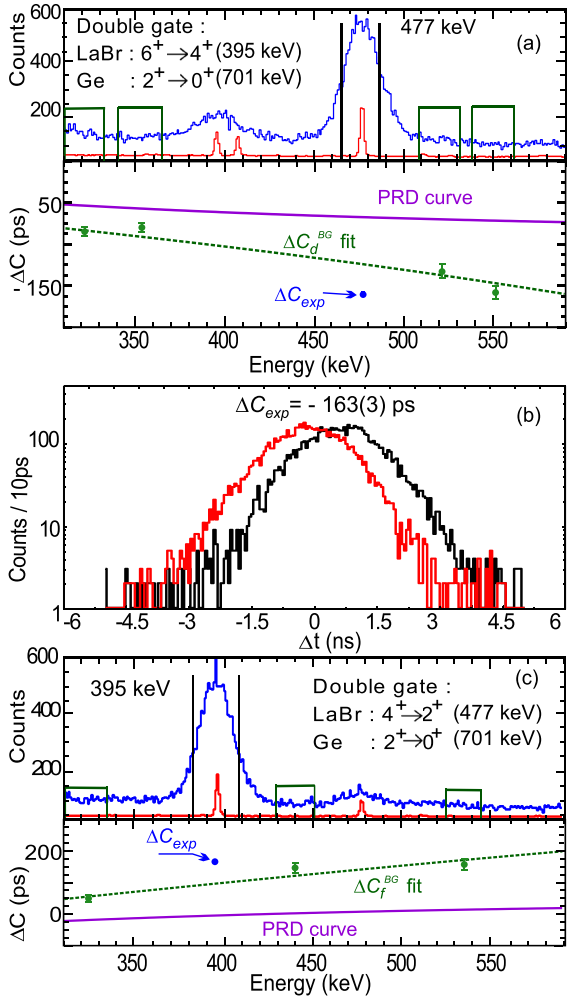

FIG. 3. The procedure for extracting the lifetime of the 4_1^+ state in ^{206}Po. (a) Double-gated spectra from LaBr (blue) detectors and HPGe detectors (red) produced from triple coincidence data by imposing the indicated coincidence conditions (gates). Here the gate on the LaBr detectors is set on the transition feeding the level of interest. The vertical black lines indicate the gate width used to produce the time-difference spectra at the full energy peak (FEP) of the decay transition. The corresponding peak-to-background ratio is 4.38. The vertical green lines indicate the gates used to extract the time response of the background. The panel below presents the fitted time response of the background (dashed green line), together with the PRD curve (magenta line) and the obtained centroid difference (the blue circle). The uncertainties of the latter is within the size of the circle. (b) LaBr delayed and antidelayed time-difference spectra for the 395- and 477-keV feeder-decay combination with additional HPGe gate on the 701-keV transition. (c) Same as (a) but the gate on the LaBr detectors is set on the decay transition. The corresponding peak-to-background ratio is 4.41. All presented spectra are not background subtracted.

In this formula, PRD stands for prompt response difference and describes the mean time-walk characteristics of the setup [19]. For the calibration of the PRD, a ^{152}Eu source was used. Two time spectra were produced by selecting feeder-decay combinations for states with well known lifetimes.

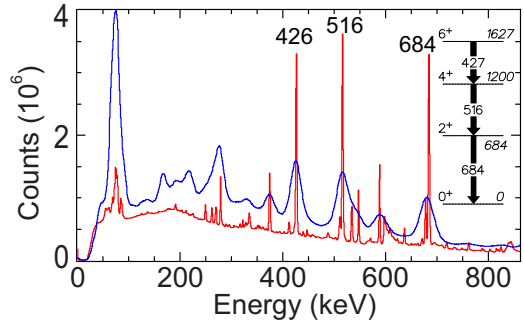

FIG. 4. Full projections of the HPGe-LaBr-LaBr (blue) and HPGe-LaBr-HPGe (red) coincidence data from the ^{197}Au(^{11}B, $4n$) reaction at a beam energy of 55 MeV. The inset shows a partial level scheme of ^{204}Po. The peaks from the transitions used in the analyses are labeled by their energies.

Measuring the centroid differences ΔC and using Eq. (1), the PRD is obtained. The data points are fitted using the function [19,20]

$$\mathrm{PRD}(E_\gamma) = \frac{a}{\sqrt{eE_\gamma^2 + b}} + cE_\gamma + d. \tag{2}$$

The final result of the PRD curve is presented in Fig. 1. The precision of the PRD fit is defined as two times the standard root-mean-squared deviation (2σ), corresponding in our case to 8 ps. More details on constructing the PRD curve for the present setup can be found in Ref. [18].

The lifetimes of interest were extracted by analyzing triple-γ coincidences. The full projections of the triple coincidences together with a level scheme of the yrast states of ^{206}Po relevant for the analysis are shown in Fig. 2. The triple-γ coincidences allow the lifetimes to be extracted from γ-γ data in LaBr detectors which are in an additional coincidence with a certain energy registered in the HPGe detectors. The latter coincidence condition improves the peak-to-background ratio in the LaBr detectors, reduces the influence of the possible contaminant transitions with energies similar to those of the feeder and/or decay transitions, and reduces the influence of the time-correlated background. The doubly gated LaBr and HPGe spectra, relevant for extracting the lifetime of the 4_1^+ state of ^{206}Po, are shown in Figs. 3(a) and 3(c). These spectra are generated from HPGe-LaBr-LaBr and HPGe-LaBr-HPGe triple coincidences data, respectively, by using the same gates in both cases. By comparing the spectra in Fig. 2 and in Figs. 3(a) and 3(c) some advantages of the triple-γ coincidences can clearly be seen. For example, the 407-keV peak which corresponds to the $2_1^+ \rightarrow 0_1^+$ transition in ^{198}Pt is clearly present in Fig. 2 and apparently cannot be resolved from the 395-keV peak in the LaBr spectra. However, once proper HPGe gates are applied, the contribution of the 407-keV peak is significantly reduced while the second LaBr gate completely eliminates it [cf. Figs. 3(a) and 3(c)].

The delayed and the antidelayed time distributions, shown in Fig. 3(b), are obtained by setting the first LaBr gate on the full-energy peak (FEP) of the 395-keV transition and

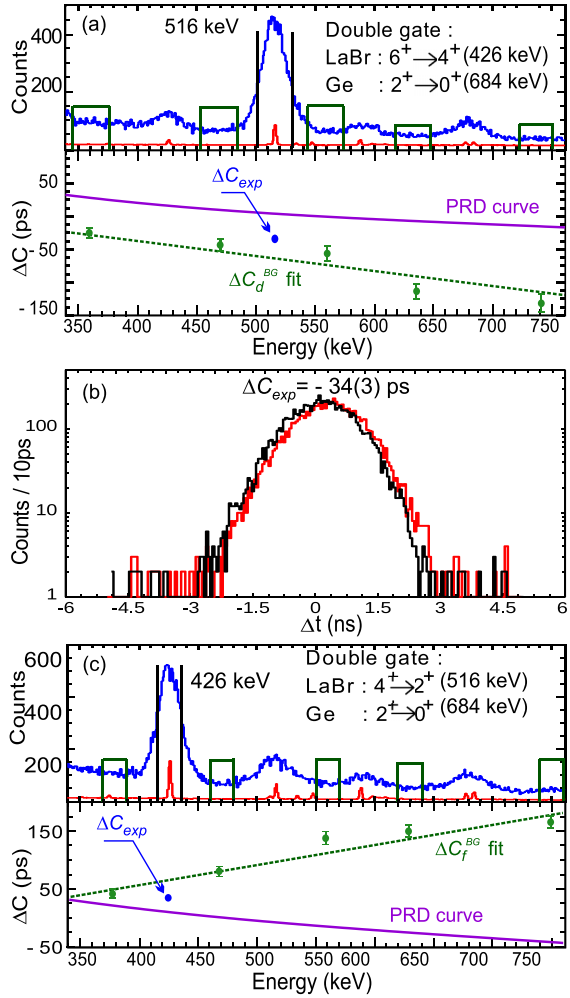

FIG. 5. The procedure of extracting the lifetime of the 4_1^+ state in ^{204}Po. The figure is analogous to Fig. 3. The corresponding peak-to-background ratios are 7.06 and 5.34.

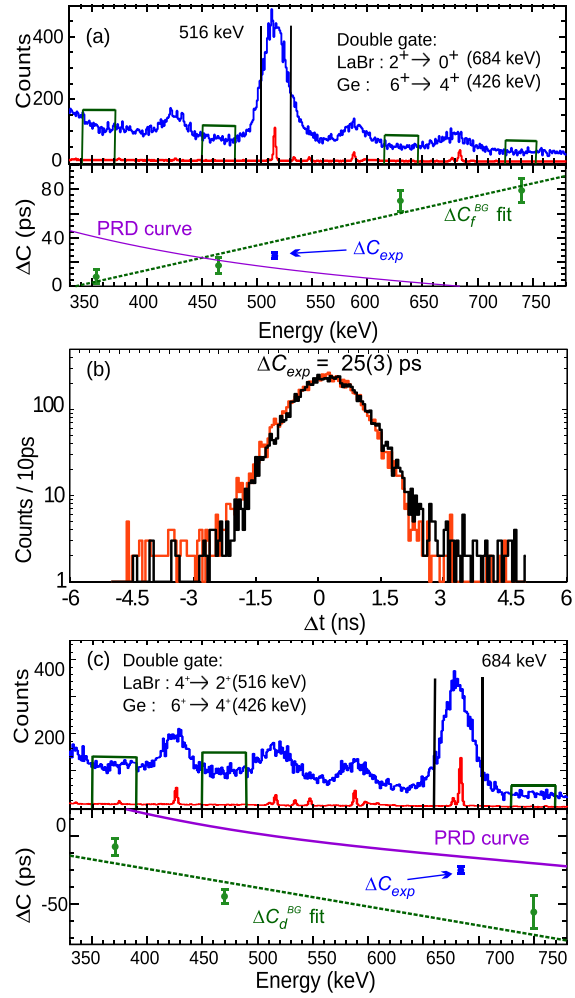

FIG. 6. The procedure of extracting the lifetime of the 2_1^+ states of ^{204}Po. The figure is analogous to Fig. 3. The corresponding peak-to-background ratios are 3.9(1) and 3.8(1).

the second LaBr gate on the FEP of the 477-keV transition. The reverse combination of gates, demonstrated in Fig. 3(c), produces the same time distributions but with exchanged "D" and "AD" labels. By measuring the difference between the centroids of these time distributions ΔC_{exp}, the lifetime can be determined. However, this value cannot be directly used in Eq. (1) since it contains contributions from the time-correlated Compton background which comes from the counts underneath the full energy peaks (FEPs). A correction for these contributions can be done by sampling the time response of the background at several positions on either side of the FEP of the decay transition [21], as depicted in Fig. 3(a). The obtained data points are fitted with a quadratic function and the time response of the background at the position of the FEP of the decay ΔC_d^{BG} is determined by interpolation. The data points used to fit the time response of the background are presented on the lower panel of Fig. 3(a). An analogous procedure is performed to obtain the time response of the background ΔC_f^{BG} at the position of the FEP of the feeder as shown in Fig. 3(c). Finally, the centroid difference ΔC which

TABLE I. Lifetimes determined from the fast-timing experiments on ^{204}Po and ^{206}Po and energies of the corresponding coincidence conditions used to obtain time-difference spectra as well as resulting $E2$ reduced transition strengths.

Nucleus	State	E_f (keV)	E_d (keV)	HPGe gate (keV)	α[a]	τ (ps)	$B(E2)(e^2\,\text{fm}^4)$
^{206}Po	4_1^+	395	477	701	0.0359	89(7)	359(28)
^{204}Po	4_1^+	426	516	684	0.0297	23(6)	939^{+326}_{-195}
	2_1^+	516	684	426	0.01584	$\leqslant 9$	$\geqslant 596$

[a]Total electron conversion coefficients for the $E2$ decay transitions. From Ref. [22].

can directly be used in Eq. (1) is calculated as suggested in Ref. [21]:

$$\Delta C = \Delta C_{\rm exp} + \frac{1}{2}\left(\frac{\Delta C_{\rm exp} - \Delta C_f^{\rm BG}}{(p/b)_f} + \frac{\Delta C_{\rm exp} - \Delta C_d^{\rm BG}}{(p/b)_d}\right), \tag{3}$$

where $(p/b)_{f,d}$ are the peak-to-background ratios observed in the gates indicated in Fig. 3. As a result of this procedure we have measured the lifetime of the 4_1^+ state of ^{206}Po to be $\tau(4_1^+; {}^{206}\text{Po}) = 89(7)$ ps.

The same analysis is used to determine the lifetime of the 4_1^+ state of ^{204}Po. The full projections of the triple coincidences, together with a level scheme of the yrast states of ^{204}Po relevant for the analysis, are shown in Fig. 4. In Fig. 5 the procedure of extracting the lifetime is presented. As in the case of ^{206}Po, here the comparison between the spectra in Figs. 4, 5(a), and 5(c) again reveals the advantages of the triple-γ coincidences. Many transitions, clearly present in the full projections in Fig. 4, are essentially eliminated in the doubly gated spectra in Figs. 5(a) and 5(c). The final result for the lifetime of 4_1^+ state of ^{204}Po is $\tau(4_1^+; {}^{204}\text{Po}) = 23(6)$ ps. It has to be noted that the larger relative uncertainty is mostly due to the smaller centroid shift difference $\Delta C_{\rm exp}$ as can be clearly seen in Fig. 5.

The lifetime of the 2_1^+ state in ^{204}Po is not known. We made an attempt to estimate it from the present data. This is illustrated in Fig. 6. The HPGe gate was set on the 426-keV transition, while LaBr gates were set on the 684- and 516-keV transitions, respectively. Thus, we were able to determine an upper limit of 9 ps for the lifetime of the 2_1^+ state in ^{204}Po. An analogous procedure in the case of the 2_1^+ state of ^{206}Po leads to a similar upper limit for the lifetime which however does not improve the precision of the $B(E2; 2_1^+ \to 0_1^+)$ value reported in Ref. [12]. The final results for the lifetimes of ^{206}Po and ^{204}Po are summarized in Table I, together with the resulting $E2$ reduced transition strengths.

III. DISCUSSION

The onset and the evolution of quadrupole collectivity in even-even nuclei are traditionally tested against four experimental criteria, namely the energy of the first excited 2^+ state $E_x(2_1^+)$, the ratio $R_{4/2} \equiv E_x(4_1^+)/E_x(2_1^+)$, the absolute transition strength $B(E2; 2_1^+ \to 0_1^+)$, and the ratio $B_{4/2} \equiv B(E2; 4_1^+ \to 2_1^+)/B(E2; 2_1^+ \to 0_1^+)$. Even though two of the criteria are uniquely defined only in several special cases of quadrupole collective excitations such as the rigid-rotor rotations ($R_{4/2} \approx 3.33$ and $B_{4/2} \approx 10/7$) and the harmonic vibrations ($R_{4/2} \approx 2$ and $B_{4/2} \approx 2$), in most cases the criteria altogether can serve well as indicators to discriminating between collective [a relatively low $E_x(2_1^+)$, $R_{4/2} \geqslant 2$, relatively large $B(E2; 2_1^+ \to 0_1^+)$ value, and $B_{4/2} \geqslant 1$] and noncollective regimes [a relatively high $E_x(2_1^+)$, $R_{4/2} \leqslant 2$, relatively low $B(E2; 2_1^+ \to 0_1^+)$ value, and $B_{4/2} \leqslant 1.5$]. However, the evolution of these observables in the chain of polonium isotopes with $N \leqslant 126$ cannot be interpreted unambiguously. Indeed, the energy of the 2_1^+ state decreases significantly from 1181 keV in $^{210}\text{Po}_{126}$ to 686 keV in $^{208}\text{Po}_{124}$ indicating that the 2_1^+ state acquires collectivity after two neutrons are removed from the $N = 126$ shell closure. However, this energy remains almost constant when more neutron pairs are removed down to $^{200}\text{Po}_{116}$ (see Fig. 1 in Ref. [12]), which is a behavior more typical for a seniority type configuration [2–4].

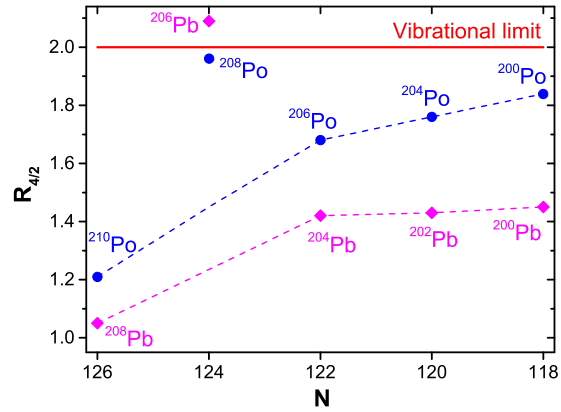

FIG. 7. The evolution of the $R_{4/2}$ ratios in even-even polonium (blue circles) and lead (magenta diamonds) isotopes as a function of neutron number. The dashed lines are drawn to guide the eye in order to highlight the peculiar $R_{4/2}$ ratio at $N = 124$ (^{208}Po and ^{206}Pb).

Experimental information on the $B(E2; 2_1^+ \to 0_1^+)$ values for the even-even polonium isotopes with $N \leqslant 126$ is scarce. This $E2$ transition strength is not known in the case of ^{208}Po but it apparently increases from 1.84(16) W.u. in ^{210}Po [23] to 18^{+14}_{-10} W.u. in ^{206}Po [12]. This rise in transition strength along with the evolution of the excitation energies of the 2_1^+ states corroborate to the conclusion that the 2_1^+ state of ^{206}Po has already a weakly collective nature [12].

In contrast, the evolution of the $R_{4/2}$ ratios presented in Fig. 7 suggests a different interpretation. It is apparent that besides the unexpectedly high $R_{4/2}$ ratio for ^{208}Po, the ratios for the other nuclei gradually increase towards the vibrational limit but still retain values typical for single-particle seniority-like excitations. The $R_{4/2}$ ratios for ^{206}Po and ^{204}Po, which are 1.68 and 1.76, respectively, agree well with the above observation. It is also worth noting that the evolution of the $R_{4/2}$ ratios in even-even polonium nuclei resembles quite closely the one

TABLE II. Available magnetic moments of the 6^+ and 8^+ states in even-even polonium isotopes with $N \leqslant 126$. Data are taken from Ref. [11].

Nucleus	^{210}Po	^{208}Po	^{206}Po	^{204}Po	^{202}Po	^{200}Po
$\mu(8_1^+)$ (μ_N)	+7.35(5)	+7.37(5)	+7.34(7)	+7.38(10)	|7.45(12)|	+7.44(16)
$\mu(6_1^+)$ (μ_N)	|5.48(5)|	+5.3(6)				

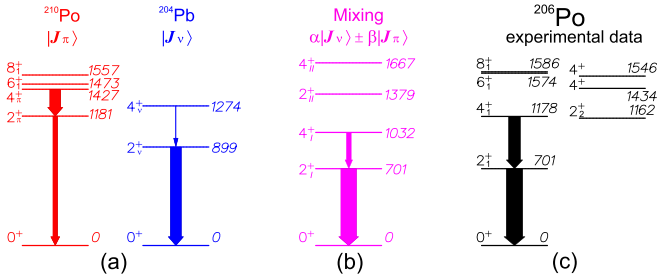

FIG. 8. The mixing scenario for ^{206}Po. Panel (a) shows the pure proton (in red) and neutron (in blue) excitations of ^{206}Po, which are assumed to correspond to the excited states of ^{210}Po and ^{204}Pb, respectively. Panel (b) shows the result from their mixing (in magenta) in comparison with experimental data for ^{206}Po in panel (c). The thickness of the arrows are proportional to the $E2$ transition strengths except for the $B(E2;2_1^+ \to 0_1^+)$ value of ^{206}Po (the rightmost level scheme), where the thickness of the arrow represents the lower limit of transition strength.

in the lead isotopes (cf. Fig. 7) including the anomaly at $N = 124$. This observation suggests that the properties of the 2_1^+ and the 4_1^+ states of polonium isotopes are predominately determined by the structures of the 2_1^+ and the 4_1^+ states of the corresponding lead nuclei which are of neutron single-particle seniority-like nature. As a result, it might be expected that the structure of the 2_1^+ and the 4_1^+ states of ^{206}Po and ^{204}Po is dominated by single-particle seniority-like configurations, which is in apparent conflict with the evolution of the $E_x(2_1^+)$ and the $B(E2;2_1^+ \to 0_1^+)$ value, as discussed above.

A solution of this ambiguity should be sought by examining the $B_{4/2}$ ratios as a last and decisive criterion for determining the nature of the 2_1^+ and the 4_1^+ states of ^{206}Po and ^{204}Po. In the case of ^{206}Po the new experimental results for the $B(E2;4_1^+ \to 2_1^+)$ values (see Table I) and the $B(E2;2_1^+ \to 0_1^+) = 1330^{+1000}_{-800}\ e^2\,\mathrm{fm}^4$ reported in Ref. [12] lead to $B_{4/2} = 0.28^{+0.48}_{-0.13}$. Despite the large uncertainties this is a rather small value. Such small $B_{4/2}$ ratios are rarely observed [24–28]. In nuclei near closed shells small $B_{4/2}$ ratios are usually interpreted as a manifestation of seniority dominated structures [4–6]. A comparison of the $B_{4/2}$ ratio for ^{206}Po and the ones for ^{210}Po [$B_{4/2} = 2.43(39)$] [23] and ^{204}Pb [$B_{4/2} = 8.1(2) \times 10^{-4}$] [29] indicates that the structure of the 2_1^+ and the 4_1^+ states of ^{206}Po may arise from a mixing of the $\pi(h_{9/2})^2$ and the $\nu(f_{5/2})^{-2}$ seniority configurations that determine the structures of the yrast states of ^{210}Po and ^{204}Pb, respectively.

A microscopic justification of the above hypothesis can be based on the fact that the Fermi levels for protons and neutrons in ^{206}Po are quite different. The valence protons are located predominantly in the $\pi h_{9/2}$ orbital just above the $Z = 82$ shell closure, while the valence neutrons occupy predominantly the $\nu f_{5/2}$ orbital below the $N = 126$ shell closure. The energy difference between these two orbitals is about 4 MeV [30]. Due to this decoupling the proton and the neutron excitations of ^{206}Po can be considered relatively independent from each other, i.e., the excited yrast states of ^{206}Po can be considered as a mixture of proton and neutron excitations, the properties of which are determined by the excited yrast states of ^{210}Po and ^{204}Pb, respectively. Since the structure of excited yrast states of ^{210}Po and ^{204}Pb in a first order approximation can be considered as being dominated by the $\pi(h_{9/2})^2$ and the $\nu(f_{5/2})^{-2}$ seniority configurations, respectively, then the excited yrast states of ^{206}Po can be considered to be a mixture of these seniority configurations for the respective angular momenta. It has to be stressed, however, that in reality the structure of excited yrast states of ^{210}Po and ^{204}Pb involve more configurations. Especially in the case of ^{204}Pb, it can be expected that configurations such as $\nu(f_{5/2}^{-1}p_{1/2}^{-1})$, $\nu(f_{5/2}^{-1}p_{3/2}^{-1})$, and $\nu(p_{3/2}^{-2})$ make significant contribution to the structures of the excited 2^+ and 4^+ states. Accounting for all possible configurations requires full scale shell model calculations, which are outside the scope of the present work. Here we simplify the problem by considering only the dominant $\pi(h_{9/2})^2$ and the $\nu(f_{5/2})^{-2}$ seniority $\nu = 2$ configurations in an attempt to obtain a qualitative understanding of the new experimental data for ^{206}Po. There is an important consequence, which follows from this approximation, namely that the described mixing produces only the 2_1^+ and the 4_1^+ states of ^{206}Po. This is a result from the fact that the $\nu(f_{5/2})^{-2}$ configuration can produce states with seniority $\nu = 2$ and spin and parity 2^+ and 4^+, while for the $\pi(h_{9/2})^2$ the $\nu = 2$ multiplet includes 2^+, 4^+, 6^+, and 8^+ states. Hence, under the above assumptions it can be expected that the yrast 6^+ and 8^+ states of ^{206}Po are dominated by the $\pi(h_{9/2})^2$ configuration, as those of ^{210}Po. This assumption is justifiable at least for the 8_1^+ states in even-even polonium isotopes, as can be seen from the constancy of the magnetic moments of these states (see Table II), which

TABLE III. Properties of the yrast states of ^{210}Po, ^{204}Pb, and ^{202}Pb used as input data for the mixing calculations for ^{206}Po and ^{204}Po.

^{210}Po[a]				^{204}Pb[b]				^{202}Pb[c]			
J_i^π	E_x (keV)	J_f^π	$B(E2;J_i \to J_f)$ ($e^2\,\mathrm{fm}^4$)	J_i^π	E_x (keV)	J_f^π	$B(E2;J_i \to J_f)$ ($e^2\,\mathrm{fm}^4$)	J_i^π	E_x (keV)	J_f^π	$B(E2;J_i \to J_f)$ ($e^2\,\mathrm{fm}^4$)
2_1^+	1181	0_1^+	136(21)	2_1^+	899	0_1^+	334(4)	2_1^+	961	0_1^+	>6.9
4_1^+	1427	2_1^+	335(14)	4_1^+	1274	2_1^+	0.272(6)	4_1^+	1382	2_1^+	20.5(15)
6_1^+	1473	4_1^+	229(7)								
8_1^+	1557	6_1^+	84(3)								

[a]The data are taken from Ref. [23] and references therein.
[b]The data are taken from Ref. [29].
[c]The data are taken from Ref. [33].

TABLE IV. Results from the mixing calculations for ^{206}Po in comparison with the experimental data. The mixing calculations are performed by using input data from Table III and $V_{\rm mix} = 308$ keV. See text for details.

Results from the mixing calculations						Experimental data			
J_i^π	$E_{x,\rm mix}$ (keV)	α^2 (neutrons)	β^2 (protons)	J_f^π	$B_{\rm mix}(E2; J_i \to J_f)$ (e^2 fm^4)	J_i^π	$E_{x,\rm exp}$ (keV)	J_f^π	$B_{\rm exp}(E2; J_i \to J_f)$ (e^2 fm^4)
$2_{\rm I}^+$	701	0.71	0.29	0^+	469(21)	2_1^+	701	0_1^+	1300^{+1000}_{-800}[a]
$2_{\rm II}^+$	1379					2_2^+	1162		
$4_{\rm I}^+$	1032	0.62	0.38	$2_{\rm I}^+$	137(5)	4_1^+	1178	2_1^+	359(28)[b]
$4_{\rm II}^+$	1667					4_2^+	1434		

[a]From Ref. [12].
[b]From the present work.

can be interpreted as due to a structure dominated by the $\pi(h_{9/2})^2$ configuration perturbed by small admixtures caused by core-polarization effects [31,32]. The fact that the magnetic moments of the 6_1^+ states of ^{210}Po and ^{208}Po are identical (see Table II) implies that these states may also be dominated by the $\pi(h_{9/2})^2$ configuration.

The mixing scenario under the above assumptions is depicted in Fig. 8. The available data for the relevant semimagic nuclei, ^{210}Po and ^{204}Pb, are summarized in Table III and are presented in Fig. 8(a). In our mixing calculations the excited states of these nuclei serve as pure proton and neutron excitations. The mixed $2_{\rm I,II}^+$ and the mixed $4_{\rm I,II}^+$ states can be expressed as $|J_{\rm I,II}\rangle = \alpha|J_\nu\rangle \pm \beta|J_\pi\rangle$ [see Fig. 8(b)], where the "+" and "–" signs are associated with the "I" and "II" labels, respectively. By imposing the condition that the energy of the lower $2_{\rm I}^+$ mixed state coincides with the energy of the 2_1^+ state of ^{206}Po, we have calculated that the effective proton-neutron residual interaction causing the mixing is $V_{\rm mix} = 308$ keV. The mixing amplitudes for the $2_{\rm I,II}^+$ states and the $B(E2; 2_{\rm I}^+ \to 0^+)$ transition strength are also calculated (see Table IV). The same quantities are calculated for the $4_{\rm I,II}^+$ states by assuming that the mixing matrix element $V_{\rm mix}$ is identical between the pure $2_{\pi(\nu)}^+$ and $4_{\pi(\nu)}^+$ states.

The results from the mixing calculations for ^{206}Po are summarized and compared to the experimental data in Table IV and in Figs. 8(b) and 8(c). The mixed $2_{\rm II}^+$ and $4_{\rm II}^+$ states appear at about 200 keV higher than any known off-yrast 2^+ and 4^+ states of ^{206}Po. In addition, there are no experimental data on the transition strengths from the off-yrast states. All this makes the unambiguous assignments of these states to any experimentally known state of ^{206}Po impossible. The mixed $2_{\rm I}^+$ and $4_{\rm I}^+$ states are neutron dominated, though the $2_{\rm I}^+$ is more pronounced (Table IV). The $4_{\rm I}^+$ state is at only 146 keV below the 4_1^+ state of ^{206}Po. The $B_{\rm mix}(E2; 4_{\rm I}^+ \to 2_{\rm I}^+)$ transition strength accounts for only about 38(3)% of the experimental value. This signals that the main assumption in the mixing calculations, namely that the excited yrast states of ^{206}Po can be considered as an admixture of the seniority $\nu = 2\,\pi(h_{9/2})^2$ and $\nu(f_{5/2})^{-2}$ configurations, are already breaking down. Apparently, the admixture of the seniority $\nu = 2\,\pi(h_{9/2})^2$ and $\nu(f_{5/2})^{-2}$ configurations cannot contribute more than 38% to the structure of the 4_1^+ state of ^{206}Po. This allows us to conclude that the structure of the 4_1^+ state of ^{206}Po is dominated by collective excitations while the contribution of the seniority $\nu = 2\,\pi(h_{9/2})^2$ and $\nu(f_{5/2})^{-2}$ configurations is secondary by size. The $B_{\rm mix}(E2; 2_{\rm I}^+ \to 0^+)$ transition strength is close to the lower limit of the experimentally determined one. Because of the large uncertainty of the experimental $B(E2; 2_1^+ \to 0_1^+)$ transition strength it is difficult to quantify to what extent the mixing calculations describe the experimental data. Even though the collective configurations may dominate the structure of the 2_1^+ state of ^{206}Po, the contribution of the admixture of the seniority $\nu = 2\,\pi(h_{9/2})^2$ and $\nu(f_{5/2})^2$ configurations is still noticeable. It is worth noting that the mixing calculations lead to a ratio $B_{4/2,\rm mix} = 0.29(2)$, which is considerably smaller than 1 and in agreement with the experimental ratio $B_{4/2} = 0.28^{+0.48}_{-0.13}$. Apparently this small $B_{4/2,\rm mix}$ ratio results from the small experimental $B(E2; 4_1^+ \to 2_1^+)$ value in ^{204}Pb (see Table III). A similar mechanism may be the reason for the low experimental $B_{4/2}$ in ^{206}Po—both 2_1^+ and 4_1^+ of ^{206}Po are collective states but the extremely low $B_{4/2}$ ratio in ^{204}Pb propagates to the low $B_{4/2}$ ratio in ^{206}Po.

We have applied the same approach to mixing calculations for ^{204}Po. This mixing scenario is depicted in Fig. 9 and the results of the calculations are summarized in Table V. In this case the properties of the pure neutron excitations of ^{204}Po are approximated by the properties of the yrast states of ^{202}Pb [see Fig. 9(a) and Table III] which are assumed to

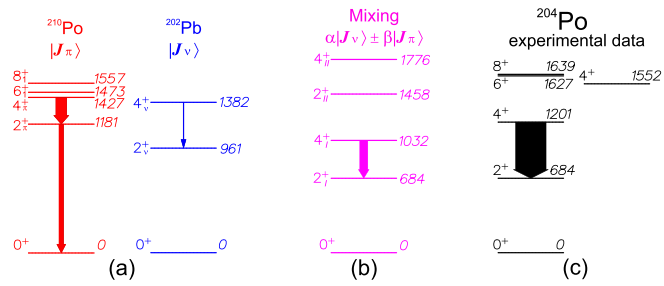

FIG. 9. The mixing scenario for ^{204}Po. Panel (a) shows the pure proton (in red) and neutron (in blue) excitations of ^{204}Po which are assumed to correspond to the excited states of ^{210}Po and ^{202}Pb, respectively. Panel (b) shows the result from their mixing (in magenta) in comparison with experimental data for ^{204}Po in panel (c). The thickness of the arrows are proportional to the $E2$ transition strengths.

TABLE V. Results from the mixing calculations for ^{204}Po in comparison with the experimental data. The mixing calculations are performed by using input data from Table III and $V_{\rm mix} = 371$ keV. See text for details.

Results from the mixing calculations						Experimental data			
J_i^π	$E_{x,\rm mix}$ (keV)	α^2 (neutrons)	β^2 (protons)	J_f^π	$B_{\rm mix}(E2; J_i \to J_f)$ (e^2 fm^4)	J_i^π	$E_{x,\rm exp}$ (keV)	J_f^π	$B_{\rm exp}(E2; J_i \to J_f)$ (e^2 fm^4)
$2_{\rm I}^+$	684	0.64	0.36	0^+		2_1^+	684	0_1^+	
$2_{\rm II}^+$	1458								
$4_{\rm I}^+$	1032	0.53	0.47	$2_{\rm I}^+$	251(9)	4_1^+	1201	2_1^+	939^{+326}_{-195}[a]
$4_{\rm II}^+$	1776					4_2^+	1552		

[a]From the present work.

be predominantly determined by the seniority $\nu = 2$ $\nu(f_{5/2})^2$ configuration. Like in the case of ^{206}Po, the properties of the pure proton excitations of ^{204}Po are assumed to be determined by the properties of the yrast states of ^{210}Po, which are dominated by the $\pi(h_{9/2})^2$ seniority $\nu = 2$ configuration. The requirement that the energy of the lower $2_{\rm I}^+$ mixed state coincides with the energy of the 2_1^+ state of ^{204}Po leads to a mixing matrix element $V_{\rm mix} = 371$ keV. Since the information of the low-lying 2^+ and 4^+ states of ^{204}Po is more scarce than the one for ^{206}Po [see Fig. 9(c)] the assignment of the mixed $2_{\rm II}^+$ and $4_{\rm II}^+$ states to any experimentally known state of ^{204}Po is also impossible (see Table V). The mixed $2_{\rm I}^+$ state is still neutron dominated but less pronounced than the one in the case of ^{206}Po. The lack of the experimental $B(E2; 2_1^+ \to 0_1^+)$ value and the impossibility to calculate the $B_{\rm mix}(E2; 2_{\rm I}^+ \to 0^+)$ value do not allow for any further insights into the structure of the 2_1^+ state of ^{204}Po. The mixed $4_{\rm I}^+$ state appears at 169 keV below the 4_1^+ state of ^{204}Po [see Figs. 9(b) and 9(c)]. This state is calculated to have essentially a balanced proton-neutron character. The $B_{\rm mix}(E2; 4_{\rm I}^+ \to 2_{\rm I}^+)$ transition strength extracted from the mixing calculations accounts only for about 27(8)% of the experimental value [see Figs. 9(b) and 9(c) and Table V]. The resemblance between the mixing calculations and the experimental data worsens from ^{206}Po to ^{204}Po even though the $B(E2; 4_1^+ \to 2_1^+)$ value in ^{202}Pb (see Table III) is by a factor of 100 larger than the one in ^{204}Pb. This is a clear indication that the main assumption in our mixing calculations is becoming increasingly invalid when the number of neutron holes increases. This implies that the contribution of the admixture of the seniority $\nu = 2$ $\pi(h_{9/2})^2$ and $\nu(f_{5/2})^2$ configurations to the excited yrast states of ^{204}Po becomes less important. Hence, the structure of the excited yrast states of ^{204}Po, or at least that of the 4_1^+ state, are dominated by collective excitations.

IV. SUMMARY

In the present study we have measured the lifetimes of the 4_1^+ states of ^{204,206}Po in an attempt to determine at what neutron number the transition from single-particle seniority-like mode to collective mode occurs. The derived absolute transition strengths were analyzed in the framework of a mixing model with the main assumption that the structure of the 2_1^+ and 4_1^+ states of these nuclei is determined by an admixture of the seniority $\nu = 2$ $\pi(h_{9/2})^2$ and $\nu(f_{5/2})^2$ configurations. Even though this is a very crude and equivocal approximation, the results from the calculations indicated that the 4_1^+ states of ^{204,206}Po are of collective nature. Based on that, we conclude that for the 4_1^+ states the transition from single-particle to collective mode occurs above neutron number 124. It has to be noted, however, that even though this conclusion seems plausible, more experimental data and more thorough theoretical investigations are needed to fully understand the process. To complete this study it is necessary to experimentally determine all missing $B(E2)$ transition strengths between yrast states of polonium isotopes from ^{208}Po down to ^{204}Po. On the theoretical side, obtaining a description of these states in the framework of large-scale shell model calculations with realistic interaction is apparently also essential.

ACKNOWLEDGMENTS

M.S. acknowledges support by the Bulgarian Ministry of Education and Science under the National Research Program "Young scientists and post-doctoral students", RD-22-862/08.04.2019. This work was supported by the partnership agreement between the University of Cologne and University of Sofia, by the Bulgarian National Science Fund under Grant No. DN08/23/2016, by the DFG under Grant No. GRK 2128, by the BMBF under Grants No. 05P18RDCIA, No. 5P18RDFN9, and No. 05P19RDFN1, and by the UK-STFC.

[1] M. G. Mayer, Phys. Rev. **78**, 16 (1950).
[2] A. de Shalit and I. Talmi, *Nuclear Shell Theory* (Academic, New York, 1963).
[3] I. Talmi, Nucl. Phys. A **172**, 1 (1971).
[4] I. Talmi, *Simple Models of Complex Nuclei: The Shell Model and Interacting Boson Model* (Harwood Academic, Chur, Switzerland, 1993).
[5] J. J. Ressler, R. F. Casten, N. V. Zamfir, C. W. Beausang, R. B. Cakirli, H. Ai, H. Amro, M. A. Caprio, A. A. Hecht, A. Heinz, S. D. Langdown, E. A. McCutchan, D. A. Meyer, C. Plettner, P. H. Regan, M. J. S. Sciacchitano, and A. D. Yamamoto, Phys. Rev. C **69**, 034317 (2004), and references therein.
[6] R. F. Casten, *Nuclear Structure from a Simple Perspective* (Oxford University Press, New York, 2000).

[7] R. F. Casten, Phys. Lett. B **152**, 145 (1985).

[8] H. Mach, A. Korgul, M. Górska, H. Grawe, I. Matea, M. Stănoiu, L. M. Fraile, Y. E. Penionzkevich, F. D. Santos, D. Verney, S. Lukyanov, B. Cederwall, A. Covello, Z. Dlouhý, B. Fogelberg, G. De France, A. Gargano, G. Georgiev, R. Grzywacz, A. F. Lisetskiy *et al.*, Phys. Rev. C **95**, 014313 (2017).

[9] K. Heyde, J. Jolie, J. Moreau, J. Ryckebusch, M. Waroquier, P. Van Duppen, M. Huyse, and J. L. Wood, Nucl. Phys. A **466**, 189 (1987).

[10] J. J. Ressler, C. W. Beausang, H. Ai, H. Amro, M. A. Caprio, R. F. Casten, A. A. Hecht, S. D. Langdown, E. A. McCutchan, D. A. Meyer, P. H. Regan, M. J. S. Sciacchitano, A. D. Yamamoto, and N. V. Zamfir, Phys. Rev. C **69**, 034331 (2004).

[11] N. J. Stone, At. Data Nucl. Data Tables **90**, 75 (2005).

[12] T. Grahn, J. Pakarinen, L. Jokiniemi, M. Albers, K. Auranen, C. Bauer, C. Bernards, A. Blazhev, P. A. Butler, S. Bönig, A. Damyanova, T. De Coster, H. De Witte, J. Elseviers, L. P. Gaffney, M. Huyse, A. Herzáň, U. Jakobsson, R. Julin, N. Kesteloot *et al.*, Eur. Phys. J. A **52**, 340 (2016).

[13] A. M. Baxter, A. P. Byrne, G. D. Dracoulis, R. A. Bark, F. Riess, A. E. Stuchbery, M. C. Kruse, and A. R. Poletti, Nucl. Phys. A **515**, 493 (1990).

[14] U. Hagemann, W. Neubert, and W. Schulze, Nucl. Phys. **175**, 428 (1971).

[15] A. Linnemann, Ph.D. thesis, Universität zu Köln, 2006.

[16] J.-M. Régis, N. Saed-Samii, M. Rudigier, S. Ansari, M. Dannhoff, A. Esmaylzadeh, C. Fransen, R.-B. Gerst, J. Jolie, V. Karayonchev, C. Müller-Gatermann, and S. Stegemann, Nucl. Instrum. Methods Phys. Res. A **823**, 72 (2016).

[17] J.-M. Régis, H. Mach, G. S. Simpson, J. Jolie, G. Pascovici, N. Saed-Samii, N. Warr, A. Bruce, J. Degenkolb, L. M. Fraile, C. Fransen, D. G. Ghita, S. Kisyov, U. Koester, A. Korgul, S. Lalkovski, N. Mărginean, P. Mutti, B. Olaizola, Z. Podolyak, P. H. Regan, O. J. Roberts, M. Rudigier, L. Stroe, W. Urban, and D. Wilmsen, Nucl. Instrum. Methods Phys. Res. A **726**, 191 (2013).

[18] M. Stoyanova, G. Rainovski, J. Jolie, N. Pietralla, A. Blazhev, M. Djongolov, A. Esmaylzadeh, L. Gerhard, K. Gladnishki, V. Karayonchev, J. Keatings, R. Kern, D. Kocheva, Th. Kröll, K. Mashtakov, O. Möller, J.-M. Régis, M. Scheck, K. Schomacker, J. Sinclair, C. ürder, V. Werner, and J. Wiederhold, Eur. Phys. J. Web Conf. **194**, 03002 (2018).

[19] J.-M. Régis, M. Rudigier, J. Jolie, A. Blazhev, C. Fransen, G. Pascovici, and N. Warr, Nucl. Instrum. Methods Phys. Res. A **684**, 36 (2012).

[20] V. Karayonchev, A. Blazhev, A. Esmaylzadeh, J. Jolie, M. Dannhoff, F. Diel, F. Dunkel, C. Fransen, L. M. Gerhard, R. B. Gerst, L. Knafla, L. Kornwebel, C. Muller-Gatermann, J. M. Regis, N. Warr, K. O. Zell, M. Stoyanova, and P. Van Isacker, Phys. Rev. C **99**, 024326 (2019).

[21] J.-M. Régis, J. Jolie, N. Saed-Samii, N. Warr, M. Pfeiffer, A. Blanc, M. Jentschel, U. Köster, P. Mutti, T. Soldner, G. S. Simpson, F. Drouet, A. Vancraeyenest, G. de France, E. Clément, O. Stezowski, C. A. Ur, W. Urban, P. H. Regan, Zs. Podolyák *et al.*, Phys. Rev. C **95**, 054319 (2017).

[22] T. Kibédi, T. W. Burrows, M. B. Trzhaskovskaya, P. M. Davidson, and C. W. Nestor, Nucl. Instrum. Methods Phys. Res. A **589**, 202 (2008).

[23] D. Kocheva, G. Rainovski, J. Jolie, N. Pietralla, A. Blazhev, A. Astier, Th. Braunroth, M. L. Cortés, A. Dewald, M. Djongolov, C. Fransen, K. Gladnishki, A. Hennig, V. Karayonchev, J. M. Keatings, J. Litzinger, C. Müller-Gatermann, P. Petkov, M. Scheck, P. Spagnoletti, Ph. Scholz, C. Stahl, R. Stegmann, M. Stoyanova, P. Thöle, N. Warr, V. Werner, W. Witt, D. Wölk, K. O. Zell, P. Van Isacker, and V. Yu. Ponomarev, Eur. Phys. J. A **53**, 175 (2017).

[24] R. B. Cakirli, R. F. Casten, J. Jolie, and N. Warr, Phys. Rev. C **70**, 047302 (2004).

[25] T. Grahn, S. Stolze, D. T. Joss, R. D. Page, B. Saygi, D. O'Donnell, M. Akmali, K. Andgren, L. Bianco, D. M. Cullen, A. Dewald, P. T. Greenlees, K. Heyde, H. Iwasaki, U. Jakobsson, P. Jones, D. S. Judson, R. Julin, S. Juutinen, S. Ketelhut *et al.*, Phys. Rev. C **94**, 044327 (2016).

[26] B. Sayg, D. T. Joss, R. D. Page, T. Grahn, J. Simpson, D. O'Donnell, G. Alharshan, K. Auranen, T. Bäck, S. Boening, T. Braunroth, R. J. Carroll, B. Cederwall, D. M. Cullen, A. Dewald, M. Doncel, L. Donosa, M. C. Drummond, F. Ertugral, S. Ertürk *et al.*, Phys. Rev. C **96**, 021301 (2017).

[27] A. Esmaylzadeh, L. M. Gerhard, V. Karayonchev, J.-M. Régis, J. Jolie, M. Bast, A. Blazhev, T. Braunroth, M. Dannhoff, F. Dunkel, C. Fransen, G. Häfner, L. Knafla, M. Ley, C. Müller-Gatermann, K. Schomacker, N. Warr, and K.-O. Zell, Phys. Rev. C **98**, 014313 (2018).

[28] B. Cederwall, M. Doncel, O. Aktas, A. Ertoprak, R. Liotta, C. Qi, T. Grahn, D. M. Cullen, B. S. Nara Singh, D. Hodge, M. Giles, S. Stolze, H. Badran, T. Braunroth, T. Calverley, D. M. Cox, Y. D. Fang, P. T. Greenlees, J. Hilton, E. Ideguchi *et al.*, Phys. Rev. Lett. **121**, 022502 (2018).

[29] C. J. Chiara and F. G. Kondev, Nucl. Data Sheets **111**, 141 (2010).

[30] E. K. Warburton and B. A. Brown, Phys. Rev. C **43**, 602 (1991).

[31] N. Bräuer, A. Goldmann, J. Hadijuana, M. Von Hartrott, K. Nishiyama, D. Quitmann, D. Riegel, W. Zeitz, and H. Schweickert, Nucl. Phys. A **206**, 452 (1973).

[32] O. Häusser, T. K. Alexander, J. R. Beene, E. D. Earle, A. B. McDonald, F. C. Khanna, and I. S. Towner, Nucl. Phys. A **273**, 253 (1976).

[33] S. Zhu and F. G. Kondev, Nucl. Data Sheets **109**, 699 (2008).